Journal of Nano- and Electronic Physics
Vol. **9** No 1, 01025(5pp) (2017)

Журнал нано- та електронної фізики
Том **9** № 1, 01025(5cc) (2017)

Resistive Switching Properties of Highly Transparent SnO_2:Fe

S.J. Trivedi, U.S. Joshi*

Department of Physics, School of Sciences, Gujarat University, Ahmedabad-380 009, India

(Received 09 December 2016; published online 20 February 2017)

Fe doped SnO_2 transparent thin film nanostructures were grown by chemical solution deposition and its electric field induced resistive switching properties were investigated for non-volatile resistive random access memory (RRAM) applications. Simple, low temperature solution process growth of SnO_2:Fe thin film nanostructures was employed. Grazing incidence X-ray diffraction (GIXRD) and atomic force microscopy (AFM), respectively, confirmed a phase pure cubic growth with mono-disperse nanocrystallites of ~ 20 nm. Sharp interface with substrate and top metal electrodes were achieved. Reproducible hysteresis in the *I-V* curves with symmetrical resistance switching ratio of more than 4×10^3 at a low operating voltage of ± 1.1 V has been demonstrated. Large values of memory retention of about 5 moths; confirmed the non-volatile behaviour of the device cell consisting of Ag/SnO_2:Fe/Ag planar structure. A mechanism involving the space charge limited current combined with Schottky conduction at the metal/oxide interface is proposed. A possible mechanism of the formation and rupture of conducting filament is proposed based on the Joule heating effect with external electron injection at the Ag/SnO_2 interface.

Keywords: Resistance switching, Tin oxide, UV, Vis spectroscopy, RRAM.

DOI: 10.21272/jnep.9(1).01025 PACS numbers: 73.61._r, 78.20._e

1. INTRODUCTION

Resistive random access memory (RRAM) is one of the candidate technologies for the promising next generation non-volatile memories with fast switching speed, low power consumption, nondestructive read out and high scalability [1-3]. The current candidate materials for RRAM devices include doped perovskites [4-5] and binary transition metal oxides such as NiO [6-7], TiO_2 [8] Cu_xO [9], ZnO [10], ZrO_2 [11], HfO_2 [12] etc. Compared with ternary or quaternary oxide semiconductor films such as doped $SrZrO_3$ or (Pr,Ca)MnO_3, binary metal oxides have the advantage of a simple fabrication process and are more compatible with complementary metal-oxide semiconductor (CMOS) processing. Further, the binary oxides being simple systems set good starting point to understand the mechanism governing the electric pulse induced resistance (EPIR) switching phenomena. Several models based on either the bulk or the interfaces effect, such as the Schottky barrier model, the filamentary model, joule heating and the model involving the dislocations from oxygen content, gross defects induced resistance switching etc. have been proposed both on experimental and theoretical frameworks [2-3], [13-18] although these mechanisms cannot fully explain the universal resistance switching (RS) behaviours. In addition, several obstacles, such as the compatibility to modern semiconductor processes, the uniformity of memory behaviour, and the retention property of RRAM devices need to be overcome before potential device applications can be considered. There is therefore a growing need to explore new binary oxides for RRAM applications.

In this paper, the memory retention behaviour of transparent Fe doped SnO_2 thin films for RRAM applications are reported. Symmetrical resistance switching (RS) with same pair of metal electrodes forming a planner Ag/SnO_2:Fe/Ag structure using four probe method is demonstrated. SnO_2 is a transparent wide-band-gap oxide semiconductor which is applied widely in many fields of oxide electronics [19-20], owing to its good optical and electrical properties and excellent chemical and thermal stability [21]. It is well known that widely-used transparent conducting oxide (TCO) thin films such as ZnO, SnO_2, SnO_2:In are *n*-type because of the existence of intrinsic defects (oxygen vacancies and/or metal interstitials) [19]. $Fe^{2+/3+}$ substitution for Sn^{4+} introduces holes in the system and annihilate part of the intrinsic *n*-type carriers and decreases the carrier density.

2. EXPERIMENTAL PROCEDURE

Nominal 5 at. wt % Fe doped SnO_2 films were synthesized by chemical solution deposition (CSD) on double side polished SiO_2 substrates. The details of film fabrication can be found in Ref. [22]. High purity (> 99.9 %, Sigma Aldrich) hydrated [$SnCl_2 \cdot 2H_2O$] and [$Fe(NO_3)_3$ $9H_2O$] were used. The solution was spun coated on clean, sonicated SiO_2 square substrates at 4000 rpm for 30 sec followed by slow drying in air at 400 °C for 1 min. This process was repeated several times to obtain the film thickness of about 160 nm. The films were annealed under oxygen flow at 650 °C for 2 hrs. All the films were characterized by grazing incidence X-ray diffraction (GIXRD), atomic force microscopy (AFM), cross section SEM and electrical properties. For electrical measurements, stripe shaped Ag electrodes of dimension 400×200 μm^2 and 100 nm thickness were deposited through metal shadow mask on the films by vacuum evaporation to form planner metal/SnO_2:Fe/metal structures and copper probes were pressed directly on the films to use as electrodes. Typical four wire technique was employed to study the current voltage characteristics by using Keithley 4200 PIV semiconductor parameter analyzer.

* usjoshi@gmail.com

3. RESULTS AND DISCUSSION

The AFM images show smooth surface morphology with RMS roughness comparable to that of the SnO_2 unit cell parameter. Average crystallite size estimated from the GIXRD and AFM are in the range of 15-20 nm. Film thickness uniformity was confirmed by cross sectional SEM images of SnO_2:Fe transparent film and is shown in Fig. 1(c). The film-substrate interface can be clearly seen. The film thickness was estimated to be ~ 230 nm. The atomic percentage of elements in the film was close to that of starting stoichiometric one, as revealed by the energy dispersive analysis of X-rays (EDAX).

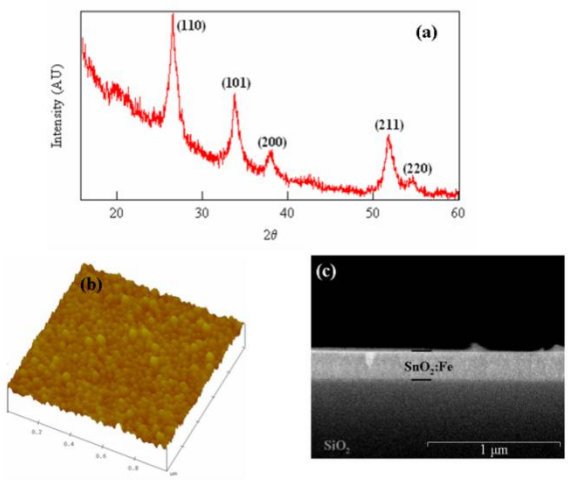

Fig. 1 – (a) GIXRD pattern of SnO_2:Fe film grown on SiO_2 substrate (b) Three dimensional AFM image (Scale 1 μm × 1 μm) and (c) Cross sectional SEM image of the film

Fig. 1 shows (a) the grazing incidence X-ray diffraction (GIXRD) pattern, (b) three dimensional AFM image and (c) cross sectional SEM image of $Fe_{0.05}Sn_{0.95}O_2$ film. All the peaks of GIXRD correspond to rutile-type phase SnO_2 nanostructure (space group $P4_2/mnm$) and the unit cell parameters were found to be $a = b = 0.51$ nm and $c = 0.946$ nm, slightly smaller than the reported ones for pristine SnO_2 films [23]. The GIXRD measurements did not reveal the existence of Fe_2O_3 or Fe_3O_4 phase, indicating that iron was incorporated into the tin oxide lattice at this doping level.

Typical current voltage (log$I$ vs. V) characteristics of Ag/SnO_2:Fe/Ag is shown in Fig. 2. The inset shows a schematic of the planar device structure used for electrical measurements. A continuous voltage sweep with a sequence $-2\text{ V} \rightarrow 0\text{ V} \rightarrow +2\text{ V} \rightarrow 0\text{ V}$ was applied thorough terminals A and D and current was measured at the points B and C, respectively. Current values for several voltage sweep cycles were recorded over a span of three to four hours to examine the reproducibility of the results and even by reversing the polarity. Nearly insulating behavior was observed in the *I-V* and only small leakage could flow through the cell up to the bias voltage of ~ ± 1.0 V. This state is defined as the high resistance state (HRS). At a forward bias voltage of 1.6 V, the current was found to jump by nearly three orders of magnitude, and material offered a resistivity of about 50 kΩ. This is defined as low resistance state (LRS) in the Fig 4(a). On sweeping the voltage from + 2V → 0, a linear *I-V* curve was traced and the cell remain in the LRS until the external bias was removed.

Further, similar trend of RS was observed while sweeping the voltage with negative polarity. These results clearly suggest that the RS is bipolar and symmetric in nature. It is interesting to note that a tremendous current increase (decrease) was observed in HRS → LRS (LRS → HRS) transitions. Maximum RS ratio (R_{high}/R_{low}) of the order of 3.4×10^3 is estimated from the hysteresis loops of the *I-V* curves. Application of the voltage sweeps for over four hours duration did not alter the switching ratio significantly, as labeled by "1st" and "2nd" sweeping cycles in Fig. 2, which were recorded after a span of four hours and the RS voltages were remained the same at ± 1.1 V suggesting an excellent symmetry in resistance switching.

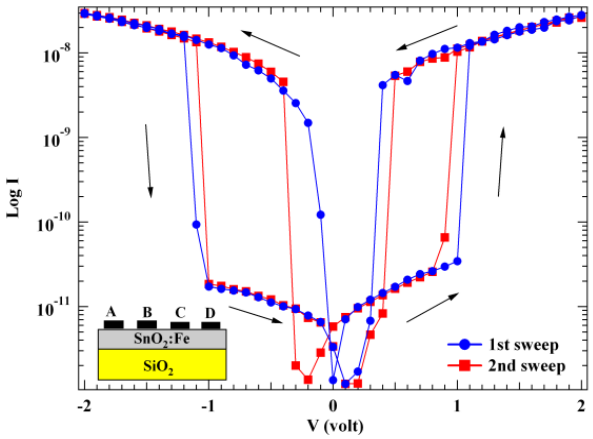

Fig. 2 – Four terminal *I–V* characteristics of Ag/SnO_2:Fe/Ag planar RRAM cell recorded just after forming the electrodes, labeled "1st sweep" and repeated after a time span of four hours, labeled as "2nd sweep". Inset shows typical measurement geometry. A continuous voltage sweep with a sequence $-2\text{ V} \rightarrow 0\text{ V} \rightarrow 2\text{ V} \rightarrow 0\text{ V} \rightarrow -2\text{ V}$, as indicated by arrows, was applied thorough terminals A and D and current was measured at the points B and C

The observed symmetry is primarily attributed to the geometry of the structure. Electrical forming process, reported in some cases of electrical-field- induced resistance switching phenomena [7-8], was not observed in any of the *I-V* characteristics. Further, the hysteresis loops are observed in I-V characteristics even by applying either forward or reverse bias to Ag electrodes in four wire geometry. This indicates that the switching is independent of bias polarities. The resistance of Ag/SnO_2:Fe/Ag planner device could be switched reversibly between HRS and LRS when pulse voltages were applied as shown in Fig. 3(a). Upon application of voltage pulses either – 2.5 V or + 3.5 V for each of 5 ms duration, the resistance was found to switch from the HRS (LRS) to LRS (HRS), respectively. The bias voltage of 0.5 V and current compliance of 0.1 A was maintained throughout the voltage sweeping cycles. The resistance switching ratio [$R_{high} - R_{low}/R_{low}$] reached nearly 430 % upon application of positive and negative pulses and was independent of the duration of pulse width up to 100 ms. Further, the resistance states are

stable without detectable signs of degradation over 600 cycles confirming the nonvolatile nature and the non-destructive readout property of the devices.

For further analysis, the retention characteristic of the device was examined to elucidate the activation of a non-volatile memory in the LRS and HRS. As can be seen from Fig. 3(b), no significant change in the resistance values in the LRS and HRS were observed up to 104 s.

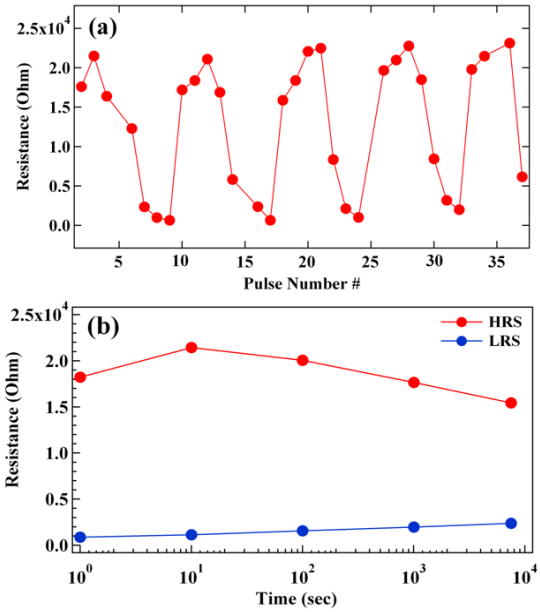

Fig. 3 – (a) Electric pulse induced resistance switching characteristics of Ag/SnO_2:Fe/Ag planar geometry (b) Retention behaviour measured at room temperature

The resistance states are stable without detectable signs of degradation over a period of 104 s, confirms the nonvolatile nature and the nondestructive readout property of the devices at room temperature. The observed memory effects and non volatility in our Ag/SnO_2:Fe/Ag planar structures are even better than the one recently reported by Nagashima et. al. [24] for Pt/SnO_2/Ti/Pt, involving stack-capacitor like device structure. These results suggest a remarkable reliability performance of Ag/SnO_2:Fe/Ag planar device cell for nonvolatile memory applications.

In order to understand the RS mechanism, we have fitted our electrical data in to well established conduction models. In the low voltage region, both the LRS and HRS curves present ohmic behaviors. Here, to clarify the mechanism governing the RS, we fitted the HRS data by using the trap-charge space charge limited current (TC-SCLC) and the Schottky conduction mechanism and the results are displayed in Fig. 4(a), where inset show the later fitting. The log I vs. log$V$ plot of Fig. 4(a) can be fitted well with a line that has a slope of 2.2, which indicates that the conduction mechanism in the HRS is static induction current (SIC) or the space charge limited current (SCLC) type. In SCLC through insulating layers, a large current increase occurs when trapping sites in the insulating layers are fully occupied at a threshold voltage, VT. Typically, VT is around 1.0 V in the initial process of resistance switching. Above the threshold voltage, current abruptly increases at first as $I \alpha V^2$ and then reaching to V^9 as can be seen in Fig. 4(a). This drastic increase in current may be induced by trap-charge space charge limiting current (TC-SCLC). Thus, when the density of thermally generated free carriers inside the SnO_2:Fe film is greater than that of the injected charge carriers, ohmic ($I \alpha V$) behavior is observed.

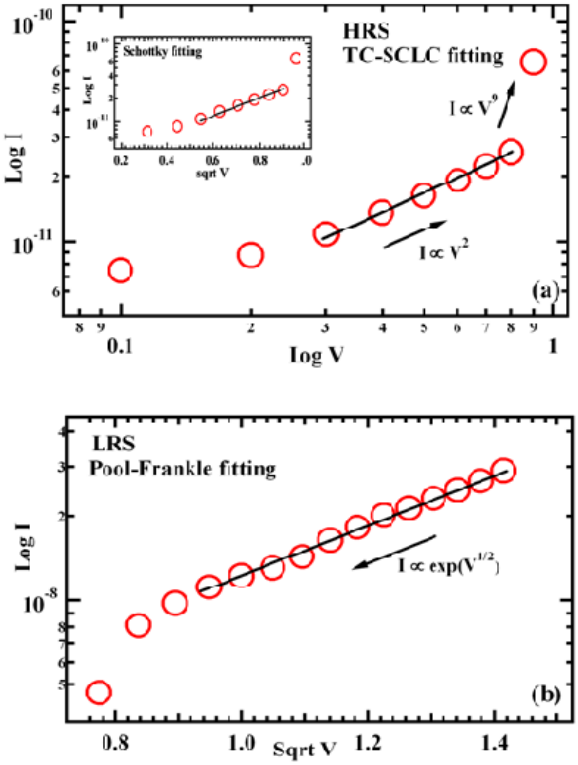

Fig. 4 – (a) Log$I$-log V plot in the HRS with TC-SCLC fitting, inset show the Schottky fitting (b) log I-$V^{1/2}$ plot fitted with Pool-Frankel equation in the LRS

Once the injected excess carriers dominate the thermally generated carriers, carrier conduction is controlled by the shallow traps ($I \alpha V^2$) represented by [9]:

$$J = \frac{9\varepsilon_r \varepsilon_o \mu V^2}{8d^3}\left(\frac{N_c}{N_t}\right)e^{-E/kT}$$

where ε_r is the static dielectric constant, ε_o is the permittivity of free space, μ is the electron mobility, V is the applied voltage, d is the film thickness, N_c is the effective density of states in the valence band, N_t is the number of shallow traps, E is the effective trapping potential, and T is the temperature. Moreover, with further increase of external bias, the observed tremendous current increase (LRS) leads to departure from the V^2 dependence to V^9 of device current, as shown in Fig. 4(a). Next, it is also suggested that the Ag/SnO_2:Fe interface may have a Schottky nature because the Schottky equation is widely used in the leakage current analysis of the metal/semiconductor structures [25]. If the Schottky conduction is obeyed in the HRS, a linear relationship between log$I$ vs $V^{1/2}$ should be obtained and the slope should give the refractive index n ($n = \varepsilon_i^{1/2}$). Inset of Fig. 4(a) show the Schottky fitting of log$I$ vs $V^{1/2}$ curves in the HRS, where linear behaviors

(slope of 2.14) are observed. The refractive index calculated from the slope is about 2.34 (with the temperature T of 300 K and thickness d of 230 nm), which is close to the value of 2.1 for SnO_2 [26]. Hence, it appears that the I-V characteristics of the Fe doped SnO_2 film are manifestations of a combined TC-SCLC and the Schottky conduction mechanism in the HRS. After switching, the I-V characteristic of the Ag/SnO_2:Fe interface is well described by the Poole-Frenkel effect ($I \alpha \exp(V^{1/2})$) and thermionic emission across the Schottky-like barrier. Indeed, the log I-$V^{1/2}$ plot in Fig. 4(b) for the LRS is a linear function above 1 V. These results suggest that both trap charged an insulating interfacial layer and a Schottky-like barrier at the Ag/SnO_2 interface are closely related to the switching phenomenon.

According to the analysis results given above, the switching of the initial SnO_2:Fe film to LRS is due to the formation of metallic filaments and/or the migration of oxygen ions close to the Ag/SnO_2 interface that accompanied by a soft breakdown. For the reset process, the resistance increases suddenly which indicates that the filamentary conducting paths might be ruptured. The Joule heating effect by the external current is considered for the rupture of filaments. By increasing the voltage to a threshold value, the high current flow through many filaments heats up the film which induces a simultaneous rupture of the filaments and the HRS is achieved [7, 13]. For the set process (LRS), it is possible to form conducting filaments by excess Sn and/or Fe ions and oxygen vacancies at the interface, because the sample stoichiometry might be perturbed under the influence of electric field. Moreover, the pulse field of the order of 105 V/cm is high enough to conceivably create dense crystalline defects through electromigration. It is well known that SnO_2:Fe, like the SnO_2:In is n-type semiconductor because of the existence of intrinsic defects (oxygen vacancies and/or metal interstitials) [19]. Recently, Ni et. al. [23] have reported p-type conductivity in SnO_2:Sb films and shown that lower valance cation substitution for Sn^{4+} works as acceptor impurity. It is therefore expected that, $Fe^{2+/3+}$ substitution for Sn^{4+} introduces holes in the system and annihilate part of the intrinsic n-type carriers and decreases the carrier density. In fact, the resistivity of the SnO_2:Fe films were found to be nearly an order of magnitude higher than that of the pure SnO_2 films (not shown). Thus, it might be possible that, both acceptor-type level and donor-type levels due to oxygen vacancies co-exist in the system. In other words, both the trapping (detrapping) of SCLC and generation (rupture) of multifilaments contribute to the carrier transport in the Ag/SnO_2:Fe/Ag device structure. Similar findings of suppression of conductivity in ZnO upon Cu doping, due to trapping of free carriers by the Cu, resulting in stable memory effect in Au/Cu-ZnO/Si stack structure has recently been reported in Ref [27]. Furthermore, Tang et.al. [28] have studied the effect of La doping on the unipolar RS behavior of ZnO, which exhibit excellent RS even in its intrinsic form [6]. Next, when the external current density is large enough in low resistance state, sufficient electrons are injected in the film and the Joule heating effect might cause a simultaneous rupture of the multifilaments. Therefore, it seems that the reset processes are resulted from the Joule heating effect.

Optical spectrograph of SnO_2:Fe film is shown in Fig. 5. Excellent transmission of better than 87 % has been observed in the entire visible range. Inset of Fig. 5 shows the absorption spectra, i.e. plot of α^2 vs. $h\nu$, where α is absorption coefficient and hv is the photon energy.

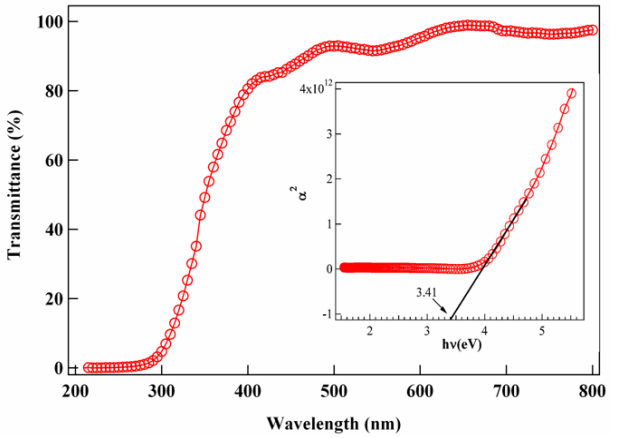

Fig. 5 – UV-visible transmission spectra of 140 nm thick SnO_2:Fe film. Inset shows the absorption spectra (α^2 *vs.* $h\nu$). The optical absorption edge was estimated to be 3.41 eV

Optical band gap (Eg) of 3.41 eV was estimated from the absorption spectra by using the relation, $(\alpha\ h\nu)^{1/2} = \text{constant}\ (h\nu - \text{Eg})$.This value is slightly higher than 3.2, reported for the SnO_2 thin film [23]. This result also suggests that Fe substitutes for Sn in SnO_2 matrix. By combining the results of resistance switching and optical properties, we have demonstrated that SnO_2:Fe is a promising candidate for transparent non-volatile RRAM device.

4. CONCLUSIONS

In summary, the resistance switching behavior of Fe doped SnO_2 transparent thin film fabricated by chemical solution deposition has been investigated for non volatile memory applications. A typical Ag/SnO_2:Fe/Ag device cell showed stable and reproducible electric-field-induced resistance switching behaviors. Non volatile memory retention having resistance switching ratio of 4×10^3 has been demonstrated. The I-V characteristics of the SnO_2:Fe film suggest that both SCLS and the Schottky conduction mechanism are important in the HRS, whereas Pool-Frankel type I-V fits well in the LRS. A possible mechanism of the formation and rupture of conducting filament is proposed based on the Joule heating effect with external electron injection at the Ag/SnO_2 interface. These results demonstrate that SnO_2:Fe has a good potential for transparent RRAM device for the next generation non-volatile memory.

AKNOWLEDGEMENTS

Authors thank Mr. Nilesh Kulkarni and Mr. R.D. Bapat, TIFR, Mumbai for their help in GXRD and cross sectional SEM measurements, respectively. Departmental support from DST-FIST and UGC under SAP is gratefully acknowledge. This work was supported by the Department of Atomic Energy (DAE-BRNS), India.

REFERENCES

1. R. Waser, A. Ono, *Nat. Mater.* **6**(11), 833 (2007).
2. A. Sawa, *Mater. Today* **11**, 28 (2008) (Kuan-Chang Chang, T. C. Chang, T. Tsai, R. Zhang, Y. Hung, Y. Syu, Y. Chang, M. Chen, T. Chu, H. Chen, C.H. Pan, C. Shih, J. Zheng, S.M. Sze, *Nanoscale Res. Lett.* 10, 120 (2015)).
3. H. Akinaga, H. Shima, *Proc. IEEE* **98**, 2237 (2010).
4. S.Q. Liu, N.J. Wu, A. Ignatiev, *Appl. Phys. Lett.* **76**, 2749 (2000).
5. A. Beck, J.G. Bednorz, C. Gerber, C. Rossel, D. Widmer, *Appl. Phys. Lett.* **7**, 139 (2000).
6. I.G. Baek, M.S. Lee, S. Seo, M.J. Lee, D.H. Seo, D-S. Suh, J.C. Park, S.O. Park, H.S. Kim, I.K. Yoo, U.-In. Chung, J.T. Moon, *Tech. Dig. Int. Electron Devices Meeting San Francisco CA* 587 (2004).
7. S. Seo, M.J. Lee, D.H. Seo, E.J. Jeoung, D.-S. Suh, Y.S. Joung, I.K. Yoo, I.R. Hwang, S.H. Kim, I.S. Byun, J.-S. Kim, J.S. Choi, B.H. Park, *Appl. Phys. Lett.* **85**, 5655 (2004).
8. B.J. Choi, D.S. Jeong, S.K. Kim, S. Choi, J.H. Oh, C. Rohde, H.J. Kim, C.S. Hwang, K. Szot, R. Waser, B. Reichenberg, S. Tiedke, *J. Appl. Phys.* **98**, 033715 (2005).
9. R. Dong, D.S. Lee, W.F. Xiang, S.J. Oh, D.J. Seong, S.H. Heo, H.J. Choi, M.J. Kwon, S.N. Seo, M.B. Pyun, M. Hasan, H. Hwang, *Appl. Phys. Lett.* **90**, 042107 (2007).
10. Y.W. Chang, Y.C. Lai, T.B. Wu, S.F. Wang, F. Chen, M.J. Tsai, *Appl. Phys. Lett.* **92**, 022110 (2008).
11. S. Kim, I. Byun, J. Hwang, J. Kim, J. Choi, B.H. Park, S. Seo, M.J. Lee, D.H. Seo, D.S. Suh, Y.S. Joung, I.K. Yoo, *Jpn. J. Appl. Phys.* **44**, L345 (2005).
12. Y.S. Chen, H.Y. Lee, P.S. Chen, P.Y. Gu, C.W. Chen, W.P. Lin, W.H. Liu, Y.Y. Hsu, S.S. Sheu, P.C. Chiang, W.S. Chen, F.T. Chen, C.H. Lien, M.J. Tsai, *Tech. Dig. - Int. Electron Devices Meeting San Francisco CA* 105–108 (2009).
13. D.H. Kwon, K.M. Kim, J.H. Jang, J.M. Jeon, M.H. Lee, G.H. Kim, X.S. Li, G.S. Park, B. Lee, S. Han, M. Kim, C.S. Hwang, *Nat. Nanotech.* **5**, 148 (2010).
14. R. Waser, R. Dittmann, G. Staikov, K. Szot, *Adv. Mater.* **21**, 2632 (2009).
15. A.A. Fursina, R.G.S. Sofin, I.V. Shvets, D. Natelson, *Phys. Rev. B* **79**, 245131 (2009).
16. B. Magyari-Kope, M. Tendulkar, S.G. Park, H.D. Lee, Y. Nishi, *Nanotech.* **22**, 254029 (2011).
17. S. Yu, H.-S.P. Wong, *IEEE Int. Memory Workshop (MTDT-2010)* 1-4 (2010).
18. U.S. Joshi, *Radiation Effects & Defects in Solids* **166**, 724 (2011).
19. D.S. Ginley, C. Bright, *MRS Bull* **25**, 15 (2000).
20. M. Batzill, U. Diebold, *Prog. Surf. Sci.* **79**, 47 (2005).
21. E. Cetinorgu, S. Goldsmith, *J. Phys. D: Appl. Phys.* **40**, 5220 (2007).
22. U.S. Joshi, S.J. Trivedi, K.H. Bhavsar, U.N. Trivedi, S.A. Khan, D.K. Avasthi, *J. Appl. Phys.* **105**, 73704 (2009).
23. J. Ni, X. Zhao, X. Zheng, J. Zhao, B. Liu, *Acta Mater.* **57**, 278 (2009).
24. K. Nagashima, T. Yanagida, K. Oka, T. Kawai, *Appl. Phys. Lett.* **94**, 242902 (2009).
25. S.M. Sze, *Physics of Semiconductor Devices*, *second ed.* (Wiley: New York: 1981).
26. V.M. Jiménez, J.P. Espinos, A. Caballero, L. Contreras, A. Fernandez, A. Justo, A.R. Gonzalez-Elipe, *Thin Solid Films* **353**, 113 (1999).
27. T. Ghosh, D. Basak, *IEEE Electron Dev. Lett.* **32**, 1746 (2011).
28. M.H. Tang, Z.Q. Zeng, J.C. Li, Z.P. Wang, X.L. Xu, G.Y. Wang, L.B. Zhang, S.B. Yang, Y.G. Xiao, B. Jiang, *Solid-State Electron.* **63**, 100 (2011).